

4. Spectral Measurements and Data Analysis

This chapter describes the spectral measurements routinely performed by the network instruments, and the methods to process final data from the instrument's raw data. The method by which the irradiance calibration of standard lamps is transferred to solar data is described in detail, followed by a description of the wavelength calibration methods. Finally, the method of calculating biological dose-rates (i.e., spectral irradiance weighted with biological action spectra) from spectral data is given.

4.1. Types of Spectral Measurements

There are five different types of instrument scans, which are routinely performed—Data, Response, Wavelength, Background, and Absolute scans. Table 4.1 gives an overview of all scans. *Data* scans measure solar irradiance while the rest are used for calibrations and quality control. *Response* scans determine system responsivity using the internal 45-Watt tungsten-halogen lamp as a source. *Internal* and *External Wavelength* scans are used to determine spectral bandwidth of the monochromator and wavelength registration utilizing mercury discharge lamps. *Background* data are continuously logged to monitor the auxiliary sensors. *Absolute* scans are performed to calibrate the system using external 200-Watt tungsten-halogen Standards of Spectral Irradiance. Finally, *User Defined* scans, i.e. scans where all scan-parameters can be specified by the instrument operator, are also performed during special events like intercomparison campaigns or site visits. All scans are described in more detail in the following sections.

Table 4.1. Spectral scans performed by the NSF Monitoring Network, 2000 revision.

Scan	Wavelength increment	Range	Approx. Duration	Approximate File Size	Interval
Data Item 1	0.2 nm	280 to 345 nm	00:04:28		
Data Item 2	0.5 nm	335 to 405 nm	00:01:56		
Data Item 3	1.0 nm	395 to 605 nm	00:03:04		
Data Item 4	0.5 nm	280 to 290 nm	00:00:17		
Total Data			13 min	7 Kbytes	15 min
Response	1.0 nm	280-605	00:05:06 per item (1 to 6 per day) plus 5 min. lamp warm-up	Up to 20 Kbytes	1 per day
Wavelength	0.1 nm	Segmented	16 min.	15 Kbytes	1 per day
Background	1 observation recorded/5 min.	N/A	< 00:00:01	Up to 73 Kbytes per day	Continuous, when other scans are not running.
Absolute	1.0 nm	250 to 700 nm	1 hour plus set-up time	20 Kbytes	Biweekly

Historically, the number of scans per day and the number of wavelengths measured per spectrum was a compromise between scientific needs, and the challenges of transmitting large blocks of data from remote locations. Communication facilities have improved over the years, and the scan schedule was adjusted accordingly. For a description of historic modes of operation, see previous network operation reports. All Volume 9 data were collected at a rate of four scans per hour. At sites inside the polar circles (Barrow, McMurdo, and South Pole), the instruments operate on a reduced scan schedule during winter darkness, typically one scan of each type (data, wavelength, and response) per day. The daily volume of data that is transferred from high latitude sites is approximately 390 Kbytes, when measurements are performed 24 hours per day. During Polar Night the file size drops to about 20 Kbytes per day. The amount of data collected in San Diego is about 250 Kbytes per day throughout the year.

4.1.1. Data Scan

Data scans measure through-monochromator PMT current caused by solar radiation. Whenever the Sun is above the horizon, they are performed every 15 minutes indexed at the top of the hour. A data scan is divided into four separate scan segments, called “items”, to allow measurements with different instrument sensitivity (i.e., different settings of the PMT high voltage) in different spectral regions. At short wavelengths (280-345 nm), the highest sensitivity (or highest PMT voltage) is applied. If this sensitivity were maintained beyond 345 nm, the instrument would saturate. Therefore, a smaller PMT voltage is applied for longer wavelengths (Items 2 and 3). A typical data scan is shown in Figure 4.1. Between 280 and 345 nm, solar data is sampled in 0.2 nm steps (Item 1); between 335 and 405 nm the wavelength increment is 0.5 nm (Item 2). Item 3 is sampled in 1.0 nm steps between 395 to 605 nm and includes most of the Photosynthetically Active Radiation (PAR) or “visible” portion of the spectrum. Wavelengths between 335 and 345 nm and these between 395 and 405 nm are measured by two different items. When items overlap, the lower item data are published.

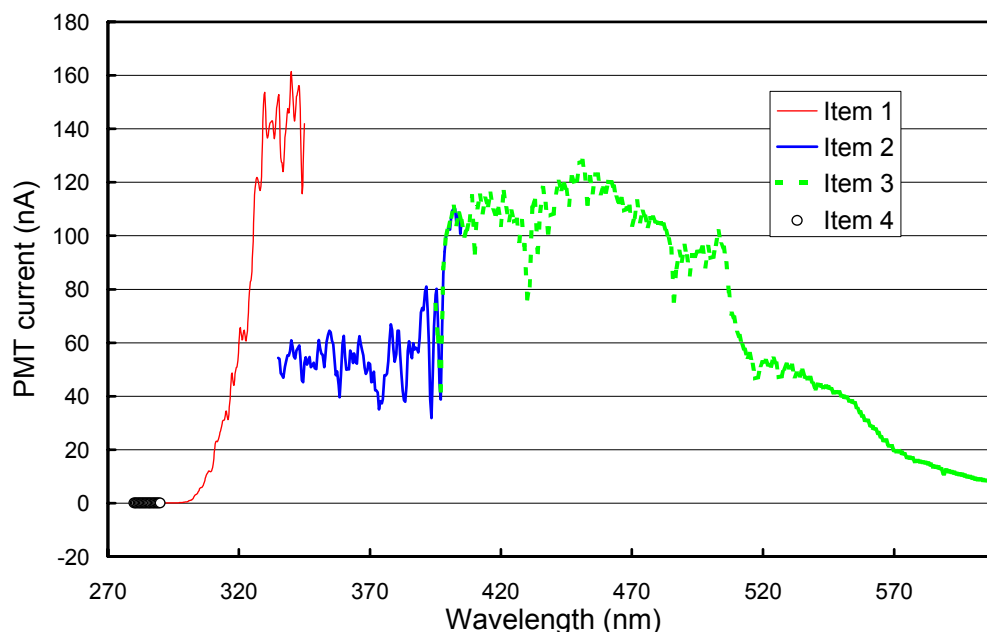


Figure 4.1. Data Scan: PMT current during solar measurements before conversion to irradiance. Item 1 covers the spectral range 280-345 nm; Item 2 335-405 nm; and Item 3 395 to 605 nm. Item 1 is measured with a higher PMT voltage than Items 2 and 3. Item 4 (280-290 nm) is a measurement of the PMT dark current with the same PMT voltage applied as during Items 2 and 3.

In the course of data evaluation, the PMT dark current (i.e., the PMT current without radiation falling on the PMT’s photo-cathode) is subtracted from the measurements (see Section 4.2.1.2.). Since there is no detectable solar radiation impinging the Earth’s surface with wavelength below 290 nm, the dark current assigned to Item 1 is simply the average of measurements between 280-290 nm calculated from the same segment. A data scan consequently also includes a fourth item; a scan from 290 to 280 nm in 0.5 nm steps carried out with the same PMT high-voltage setting as for the Items 2 and 3. Since the PMT dark currents are measured with the shutter open, stray light (e.g., photons with wavelengths above 290 nm that are registered at smaller wavelengths) may also fall on the PMT cathode. Systematic errors in the measurement due to stray light (if present), are therefore partly reduced when subtracting the dark current.

At the beginning of Item 1 and Item 2, a delay of about 1-minute is specified to allow the PMT to stabilize at the new high voltage setting. A typical data scan takes about 13 minutes to complete. Figure 4.2 shows the approximate relationship between time and wavelength. This function may slightly change from scan to scan, and is also slightly different for each site. The start time of Item 1 is listed for each data scan in the field “TimeA” of the published Database 1. Similarly, the start of Item 2 is given in the field “TimeB” of Database 2. Start time of item 1 and end time of item 3 are also given in the header of composite scans.

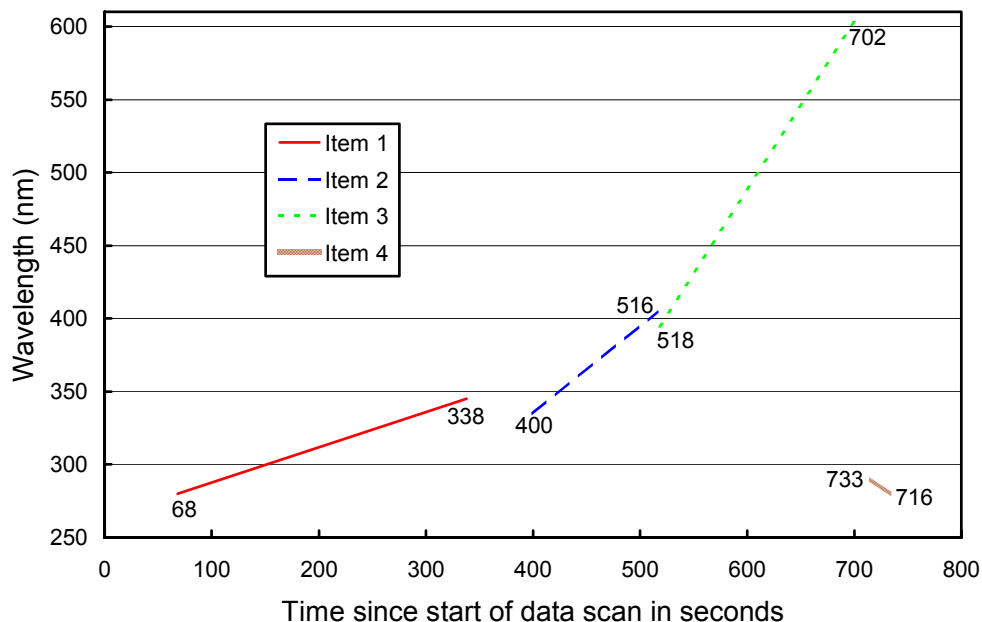


Figure 4.2. Relationship of time at start of a data scan and measured wavelength for all four items of a data scan. The data are from the instrument in San Diego. The numbers are start and end time of the different items in seconds. Note that item 4 goes from 290 to 280 nm rather than from 280 to 290 nm.

The PMT high voltage setting of data scans is diurnally optimized to produce a maximum dynamic range without overload. These automatic adjustments can result in the use of one to six different PMT high-voltage sets per day, dependent on time-of-year and location. Spectral irradiance values, calculated from the data scan, are displayed in Figure 4.3 (linear y-axis) and Figure 4.4 (logarithmic y-axis).

Since the start of network operation in 1988, several changes have been made to the data scan. The item 2 segment upper limit was increased first from 350 nm to 380 nm (1994-95), and again to 405 nm (1996) to further increase scan-resolution of the UV-A to visible band. These extensions required reductions in sensitivity to avoid saturation. The slight loss of sensitivity when the segment was extended up to 405 nm in 1996 was partly compensated for by introduction of a new feature into the SUV-100 System Control Software that allows diurnal changes in PMT high voltage as a function of solar zenith angle. This resulted in maintenance of an optimum sensitivity throughout the day. The terminal wavelength for the item 3 scan was also reduced from 700 to 620 nm (1994-95) and again to 605 nm (1996). The system sensitivity at wavelengths longer than 600 nm is poor due to the monochromator and PMT optimization for the ultraviolet. In examining the data, we found that this sensitivity was so poor that we advise users to ignore data beyond 600 nm. A change to the wavelength increment of the Item 3 segment was in response to requests of data users. In the 1991-1992 season, the increment was changed from 5 nm to 2.5 nm, and during the 1992-1993 season, it was further reduced to 1 nm.

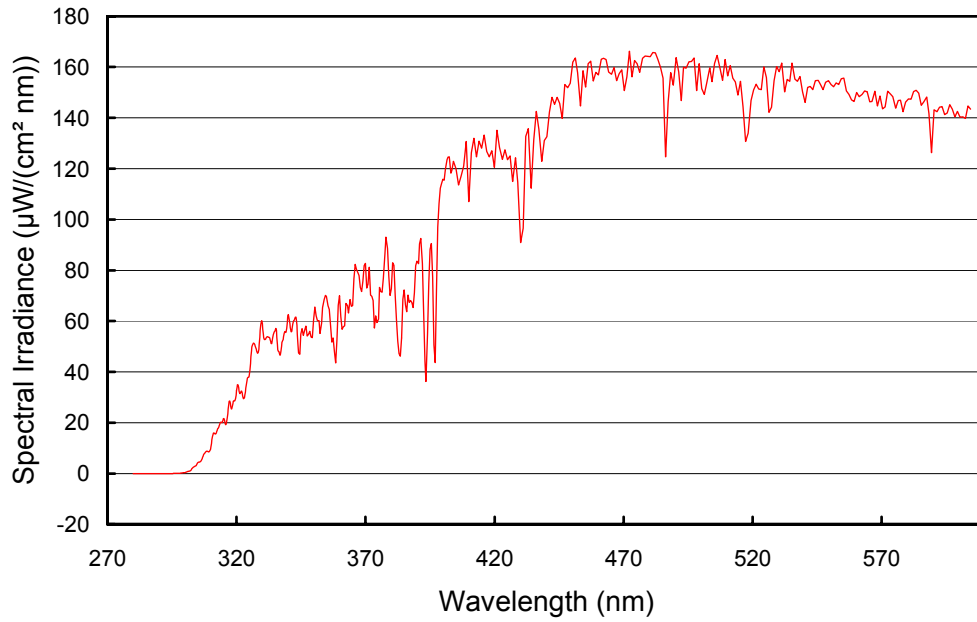


Figure 4.3. Irradiance calculated from the PMT currents shown in Figure 4.1. Data from all three scan items are included.

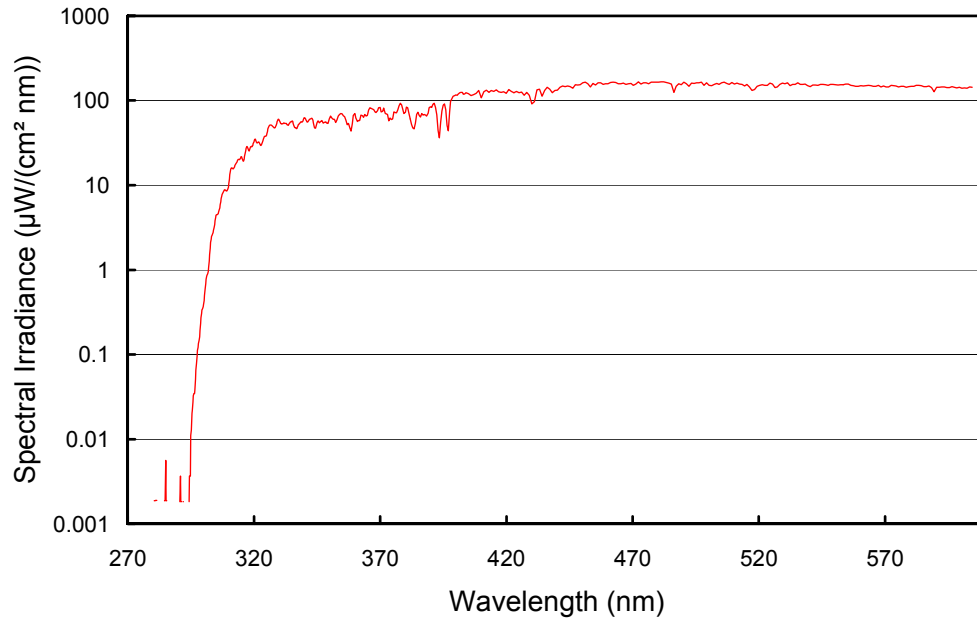


Figure 4.4. Spectral irradiance from the previous figure but presented on logarithmic y-axis to demonstrate the steep decline of the solar spectrum in the UV-B. The spikes between 280 and 290 nm indicate the detection limit of the instrument, which is caused by signal noise.

4.1.2. Response Scan

Response scans measure the PMT current when the internal 45-Watt tungsten-halogen lamp of the SUV-100 is energized. They are typically performed once per day. Response scans track changes in the system responsivity and are used for adjustment of the instrument calibration. As mentioned above, the data scan PMT high voltages are automatically adjusted as a function of solar zenith angle in order to optimize system responsivity throughout the day. A response scan consists of several items with different PMT high voltages applied, which match the voltages used during that day's data scans. Prior to initiating the scan segment(s), an adequate lamp stabilization period following power-up ensures that the lamp reaches thermal equilibrium before the scan. After the "warm-up" period, the lamp drive current is then adjusted to a target setting and accurately controlled (see Section 2.1.2). Figure 4.5 shows typical data recorded from a response scan. The lines represent PMT currents as a function of wavelength for a six-item response scan, at the various sensitivities (PMT high voltages) used in a single diurnal cycle. For quality control purposes, TSI sensor readings and the response lamp drive current are also recorded during the response scan. These parameters are reviewed to ensure that there are no response lamp changes during these scans.

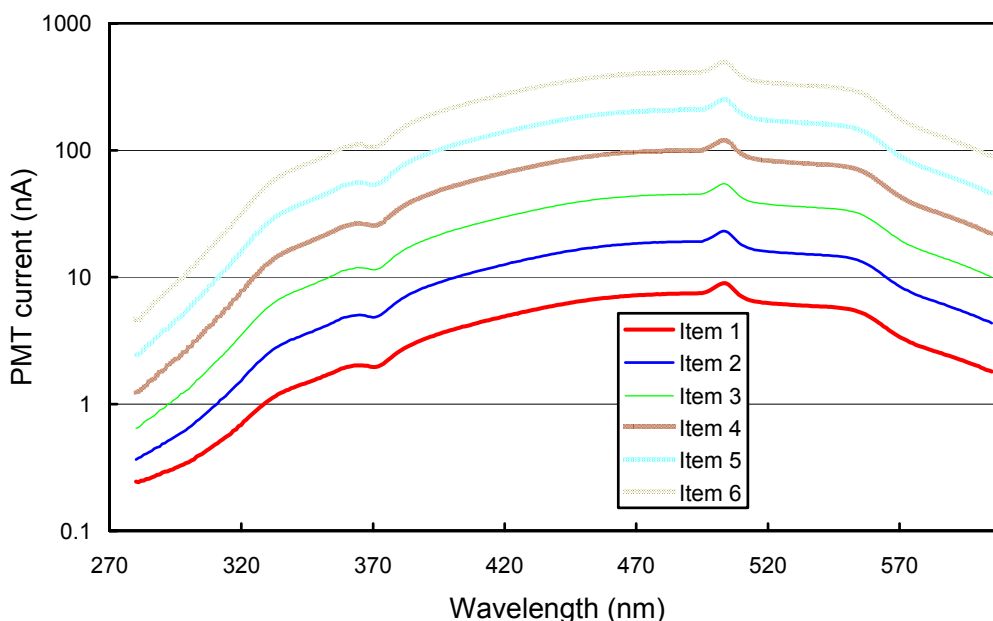


Figure 4.5. Six-item response scan. Note that PMT dark current is not subtracted.

4.1.3. Internal Wavelength Scan

Wavelength scans with the built-in mercury lamp are carried out in order to align the wavelength position of the system to the actual wavelength of photons passing the monochromator. In addition, wavelength scans allow to identify changes in the bandpass (or bandwidth) of the monochromator. Usually one wavelength scan per day is scheduled. The wavelength scan is composed of a series of segments, with the shutter closed and internal mercury discharge lamp energized. Segments are chosen to concentrate high spectral resolution scanning in areas throughout the spectroradiometer's sensitive range, where significant mercury lines occur. The PMT high voltage settings for each segment are optimized to maximize the signal observed at the peaks of the mercury lines, and to maximize signal-to-noise ratio and linearity without saturation of the PMT. The band shape of a typical 253.65 nm segment resembles that shown in Figure 4.6. A malfunctioning of the monochromator would distort the shape of the line, causing side lobes resembling smaller peaks. A normal multiple-item scan is shown in Figure 4.7.

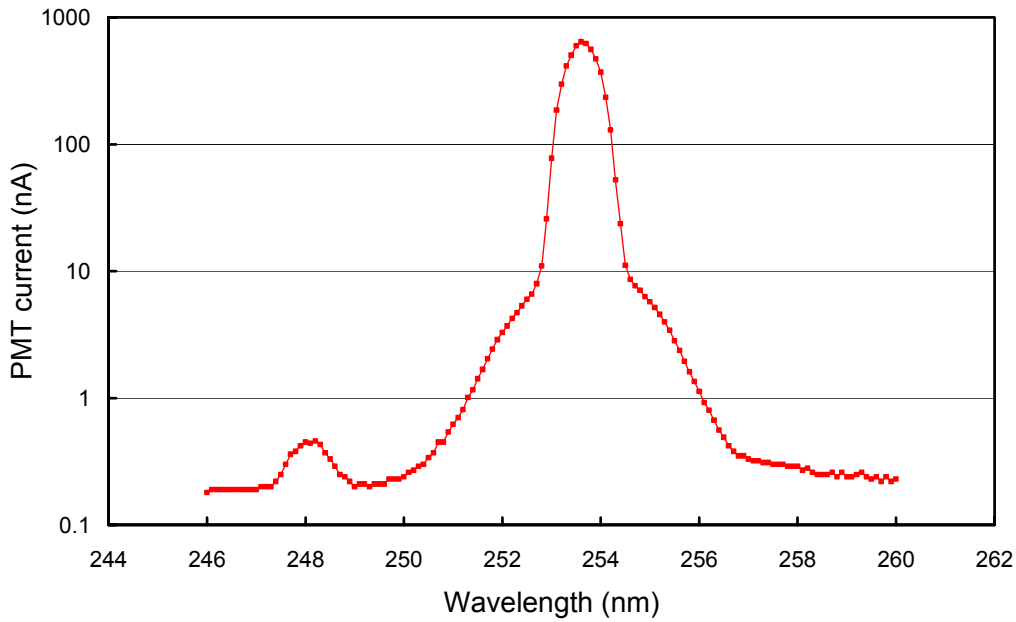


Figure 4.6. Wavelength scan in the vicinity of the mercury peak at 253.65 nm. Points indicate the individual measurements. Note that no dark value has been subtracted, and the data has not been corrected for the monochromator offset. The small peak at 248 nm is from a weaker mercury line.

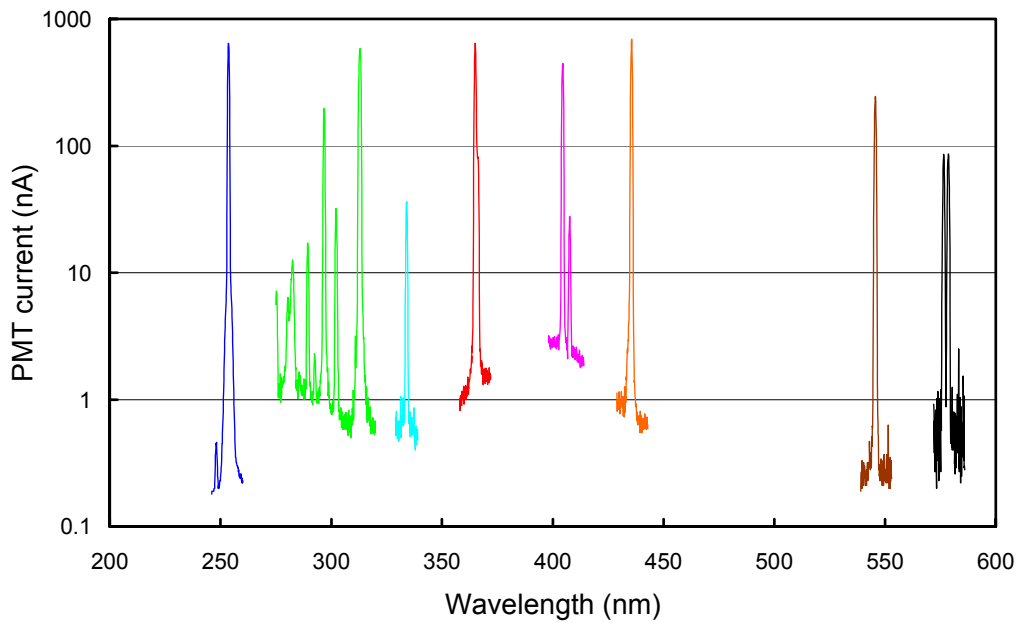


Figure 4.7. Typical multi-peak Wavelength Scan showing eight segments. In a typical wavelength scan, the baseline value may show variation across the spectrum due to fluorescence from the lamp. Note that PMT dark current has not been subtracted.

4.1.4. External Wavelength Scan

We determined at the Boulder, Colorado 1994 intercomparison (Thompson et. al., 1997) that wavelength scans performed with internal and external sources differ due to different light paths for both scan types. Radiation from the internal mercury lamp passes through two beam-splitters and enters the monochromator's entrance slit without further scattering. Radiation from an external mercury lamp is scattered first by the cosine collector before it enters the monochromator. Due to the different light path geometries the monochromator's gratings are illuminated differently causing the deviation observed in the wavelength registration. Beginning with the site visits of the 1994-1995 season, external wavelength scans have been performed as a routine part of the site visit. These scans provide a realistic measurement of the systems' bandpass and wavelength mapping, as the light path of external scans is the same as that for solar irradiance measurements.

During the external wavelength scan, a mercury lamp is situated so that it fills the entire field-of-view of the collector. The external wavelength scan is composed of a series of items that are spectrally identical to internal wavelength scan segments. A comparison of typical external and internal mercury scans is shown in Figure 4.8. The wavelength scale of the figure is the same as applied in published solar data of Volume 9. The peaks of the external scans, which has the same light path as solar measurements, agree well with the nominal wavelength of 296.73 nm, whereas the peaks of the internal scans are shifted about 0.12 nm to shorter wavelengths. External scans have a bandwidth of about 1.0 nm FWHM, whereas the bandwidth of the internal scan is typically 0.75 nm. Until the release of Volume 6 data, no attempt was made in the data processing to correct for these effects, i.e., the wavelength mapping was solely based on internal scans; external scans were only used for documentation. Starting with Volume 7, a different method for wavelength calibration was implemented, which is described in Section 4.2.2.2. Figure 4.8 also shows that measurements performed in 1998 and 1999 are very reproducible. This demonstrates the good stability of the system.

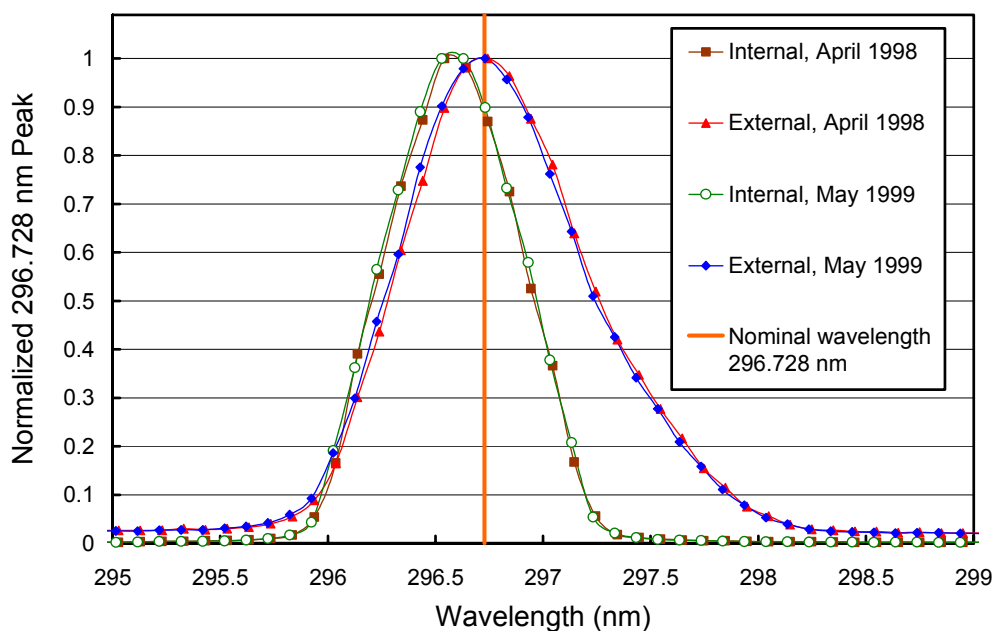


Figure 4.8. Normalized mercury peaks from external and internal wavelength scans. Data is from Palmer Station. The comparison of data from 1998 and 1999 demonstrates the good stability of the system.

4.1.5. Absolute Scan

The purpose of absolute scans is to transfer the irradiance scale from 200-Watt tungsten-halogen Standards of Spectral Irradiance (“site standards”) to the internal 45-Watt irradiance reference lamp. In addition, absolute scans are sometimes used to compare different 200-Watt standards, and to calibrate spare lamps. Under normal circumstances, i.e., when the system is stable and operating properly, these scans are performed biweekly. In order to perform an absolute scan, the 200-Watt lamp is positioned in a specially designed lamp stand outside the roof box such that the distance from the lamp filament to the diffuser of the SUV-100 spectroradiometer collector is 50 cm, as specified in the calibration certificate of the 200-Watt lamp (see Section 2.1.2 for details).

Figure 4.9 shows a typical absolute scan. This scan consists of eight segments, where the first four items characterize system behavior at short wavelengths (250-330 nm), and the last four segments characterize behavior between 250 nm and 700 nm. The reason for having two sets of four items is to optimize the system sensitivity via PMT high voltages for different parts of the spectrum. Items 1 through 4 are run at the same PMT high voltage setting, and 5 through 8 are run at a lower high voltage setting. Each of the two sets has the following segments:

- Items 1 and 5 are performed with the lamps turned off and the shutter open; it measures PMT dark current for the following 200-Watt lamp scan and detects any light leaks.
- Items 2 and 6 measure PMT current with the 200-Watt lamp on and the shutter open.
- Item 3 and 7 measure PMT current with the 45-Watt lamp on and the shutter closed.
- Item 4 and 8 measure PMT dark current with the lamps turned off and the shutter closed.

A warm-up time of 6 minutes is applied preceding measurements of both lamps.

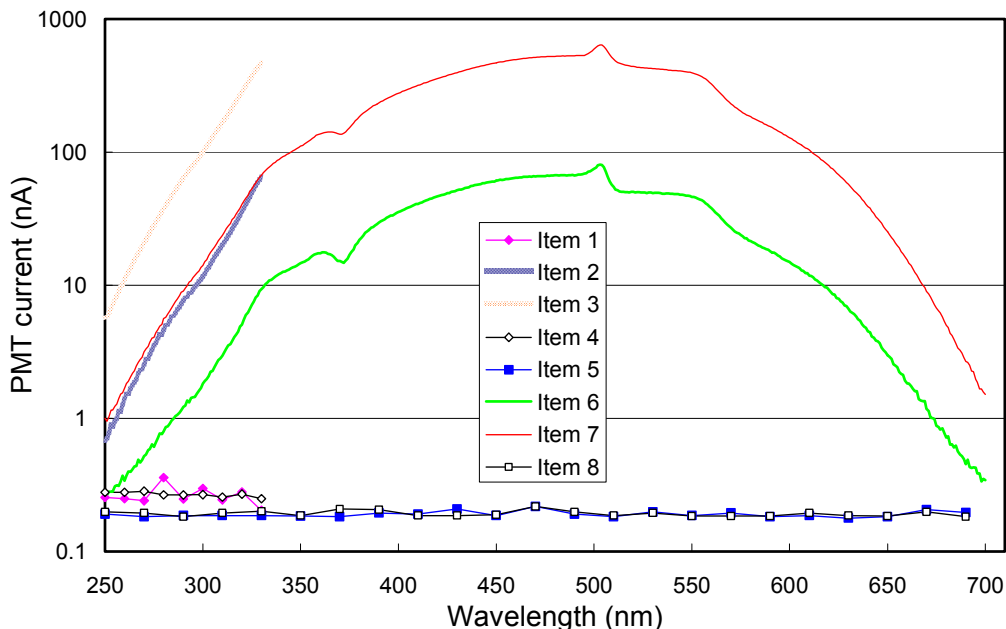


Figure 4.9. Typical eight-item absolute scan.

4.2. Calibration and Data Processing

This section describes the method used to calculate global spectral irradiance, biologically weighted dose-rates and daily doses from raw wavelength and PMT current data generated by the spectroradiometers. The irradiance calibration of data scans is explained in Section 4.2.1.; the wavelength calibration of the instruments is described in Section 4.2.2.

4.2.1. Irradiance Calibration

At each instrument site, an irradiance (or absolute) calibration is performed approximately biweekly to transfer a calibration to the internal irradiance reference lamp. This section describes how:

- The calibration certificate values of 200-Watt Standards of Spectral Irradiance are interpolated (Section 4.2.1.1.)
- The internal irradiance reference lamp is calibrated (Section 4.2.1.2.)
- The system responsivity is determined, and solar data is calibrated (Section 4.2.1.3.)
- 200-Watt standards are intercompared (Section 4.2.1.4.)
- A calibration is transferred from one 200-Watt standard to a second one (Section 4.2.1.5.)

Most quantities used for these calculations are defined in Table 4.2.

Table 4.2 Data processing parameters.

V	PMT high voltage setting for the photomultiplier tube (PMT)
λ	Wavelength
$I_{\text{dark}}(V)$	Mean PMT dark current for a given PMT high voltage
$I_{\text{ext}}(\lambda, V)$	PMT current during an absolute scan utilizing external standards
$I_{\text{int}}(\lambda, V)$	PMT current during a scan of the internal irradiance reference lamp
$I_{\text{solar}}(\lambda, V)$	PMT current during a solar data scan
$E_{\text{interp}}(\lambda)$	Interpolated irradiance values of a 200-Watt Standard of Spectral Irradiance calculated from the (NIST-traceable) calibration certificate of that lamp
$E_{\text{int}}(\lambda)$	Apparent irradiance of the internal irradiance reference lamp as a function of wavelength
$E_{\text{solar}}(\lambda)$	Solar irradiance as a function of wavelength
$R(\lambda, V)$	System responsivity

The following may influence a correct irradiance calibration:

1. A 200-Watt standard of spectral irradiance has changed its intensity between its factory calibration and its use on-site.
2. The entrance optics or other system components have changed between calibrations with 200-Watt lamps.
3. The internal irradiance standard lamp has changed.
4. Other instrument deficiencies.

Using two or more different lamps on-site minimizes uncertainties because of (1). Additionally, a traveling Standard of Spectral Irradiance is brought to the site during annual site visits and the calibrations of all lamps are intercompared. Results of the biweekly 200-Watt calibrations are used to assess changes in the entrance optics and/or other system components, and to adjust the system responsivity accordingly. The stability of the internal response lamp is tracked by the external 200-Watt calibrations. It is additionally monitored by the TSI sensor, and drive current during operation of the lamp.

4.2.1.1. Interpolation of Values from Calibration Certificates of 200-Watt Standards

The irradiance calibration of the spectroradiometers is based on Standards of Spectral Irradiance purchased from Optronic Laboratories. These are 200-Watt tungsten-halogen lamps of type Q6.6AT4/5CL manufactured by General Electric. Their calibration is traceable to the National Institute of Standards and Technology (NIST). The lamps are calibrated by Optronic Laboratories in an apparatus geometrically identical to that used at the sites, both in lamp orientation (downward light path) and lamp-to-collector distance. To calibrate an SUV-100 spectroradiometer, the 200-Watt lamps are mounted bi-weekly on top of the instrument and scanned (see Sections 2.1.2 and 4.1.5).

The Standards of Spectral Irradiance are provided by Optronic Laboratories with a table of irradiance values in 10-nm increments. To provide irradiance values in smaller wavelength increments, for application at wavelengths obtained during the calibrations, a Black-Body function (or Planck equation) is used:

$$E_{\text{interp}}(\lambda) = a \frac{2hc^2}{\lambda^5} \frac{1}{\exp\left\{\frac{hc}{k\lambda T}\right\} - 1}$$

where h is Planck's constant, c is the velocity of light, k is the Boltzmann constant, T is the temperature in Kelvin and $E_{\text{interp}}(\lambda)$ is the interpolated spectral irradiance. The term a is a scale factor. An equation fitting routine is used to adjust terms a and T for the values provided from 290 to 600 nm to yield the best fit to Optronic Laboratories' (NIST-traceable) data, as shown in Figure 4.10.

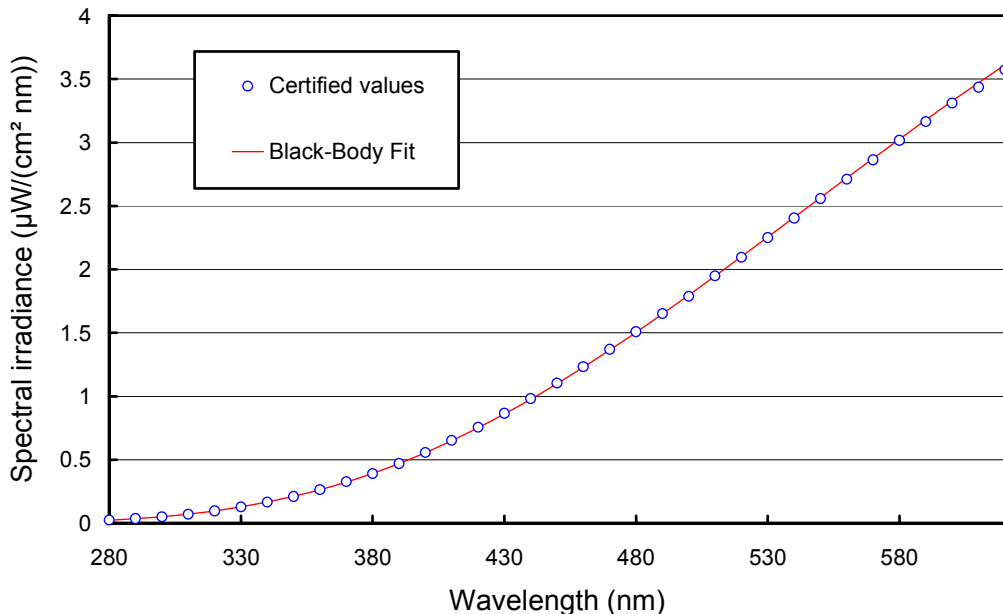


Figure 4.10. Spectral Irradiance of the standard 200W010. The open circles are the values from the lamp's certificate provided by Optronic Laboratories. The line through these points is the Black-Body fit.

Since a lamp spectrum is not a true Black-Body function, the fit will introduce an error, which is generally less than $\pm 1\%$. Figure 4.11 shows the ratio of the Black-Body fit values and the certified values of lamp 200W010. Both data sets agree to within $\pm 1\%$, indicating that the fit method chosen is reasonably accurate.

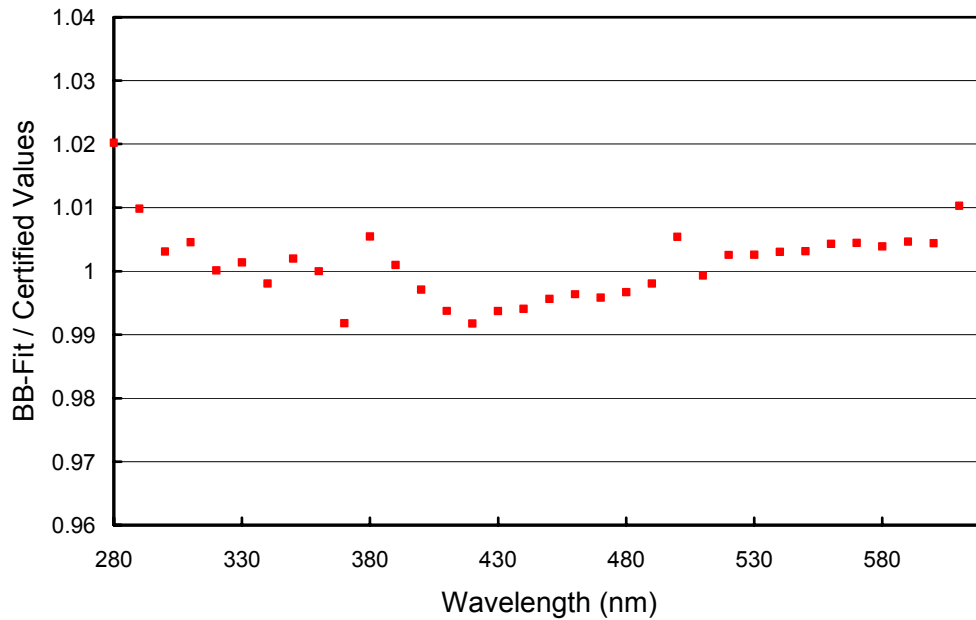


Figure 4.11. Ratio of the Black-Body fit values and the certified values of lamp 200W010. Both data sets agree to within $\pm 1\%$. The graph is based on the same values as shown in the previous figure.

4.2.1.2. Calibration of the Internal Irradiance Reference Lamp

A system irradiance calibration is established by analyzing absolute scans (see Section 4.1.5). The procedure transfers the irradiance scale from the 200-Watt Standard of Spectral Irradiance to the internal 45-Watt irradiance reference lamp. The irradiance $E_{\text{int}}(\lambda)$ assigned to the reference lamp is calculated with this formula:

$$E_{\text{int}}(\lambda) = E_{\text{interp}}(\lambda) \frac{I_{\text{int}}(\lambda, V) - I_{\text{dark}}(V)}{I_{\text{ext}}(\lambda, V) - I_{\text{dark}}(V)}$$

where $I_{\text{int}}(\lambda, V)$ is the PMT current of the internal lamp measured during Item 3 and 7 of an Absolute Scan. The PMT current when measuring the 200-W lamp, $I_{\text{ext}}(\lambda, V)$, is derived from Items 2 and 6 of the Absolute Scan. From both currents, PMT dark current $I_{\text{dark}}(V)$ is subtracted. $E_{\text{interp}}(\lambda)$ is the interpolated irradiance of the 200-Watt lamp, calculated in the previous section. An absolute scan is usually preceded by a wavelength scan, which is used to correct the wavelength scale of the scan before the above formula is applied. Note that $E_{\text{int}}(\lambda)$ is not a “true” irradiance produced by the internal lamp at the place of the entrance optics but acts as a reference value when comparing the irradiance produced by the 200-Watt standard and solar irradiance.

Each biweekly calibration with a 200-Watt Standard of Spectral Irradiance provides a function $E_{\text{int}}(\lambda)$. Ideally, these functions would not change from one calibration event to the next. In practice, there are changes due to:

- The response lamp drifted, i.e., the lamp became darker or brighter.
- Calibrations are performed with different 200-Watt standards.
- Random changes in the physical alignment of the 200-Watt standards, the supplied lamp current, or the lamp itself.

For these reasons, calibration of the spectroradiometer in a given time period is not based on one calibration event only. An average irradiance $\langle E_{\text{int}}(\lambda) \rangle$ of the internal lamp is calculated from n calibrations performed in time-intervals ranging from days to several months, depending on the stability of the response lamp:

$$\langle E_{\text{int}}(\lambda) \rangle = \frac{1}{n} \sum_n E_{\text{int},n}(\lambda)$$

In the following, $\langle E_{\text{int}}(\lambda) \rangle$ is denoted “mean-irradiance of the internal lamp”. By this averaging, the influence of differences in the 200-W standards, and random errors, are reduced. If a response lamp drifts however, the number of scans contributing to the average has to be limited in order to avoid systematic errors. The allowed drift of the lamp is typically 2%. If the drift in a given period is larger, the period is broken in two or more parts with a single mean-irradiance calculated for each part.

4.2.1.3. Determination of the System Responsivity and Calibration of Solar Data

The calculation of solar spectral irradiance at a particular time requires a data scan, a response scan, and a wavelength scan. Response and wavelength scans are typically taken from the same day as the data scan or those scans closest in time to the data scan. In the first step, data and response scan are shifted in wavelength based on the wavelength scan and a table, which defines the monochromator non-linearity. For Volumes 1- 6, this table was based on internal wavelength scans, see Section 4.2.2.1.; for Volumes 7 through 9, it is based on the Fraunhofer-correlation method described in Section 4.2.2.2. After all scans have been wavelength corrected, the responsivity R of the spectroradiometer is calculated:

$$R(\lambda, V) = \frac{I_{\text{int}}(\lambda, V) - I_{\text{dark}}(V)}{\langle E_{\text{int}}(\lambda) \rangle}$$

Note that R is determined separately for each PMT high voltage setting. $I_{\text{dark}}(V)$ is calculated from the 280-290 nm portion of the data scan. The denominator $\langle E_{\text{int}}(\lambda) \rangle$ is the response lamp’s mean-irradiance, defined in the previous section.

The solar spectral irradiance, E_{solar} , is calculated from the PMT currents $I_{\text{solar}}(\lambda, V)$ of the data scan:

$$E_{\text{solar}}(\lambda) = \frac{I_{\text{solar}}(\lambda, V) - I_{\text{dark}}(V)}{R(\lambda, V)}$$

A typical solar irradiance spectrum created with this procedure has already been shown in Figure 4.3.

4.2.1.4. Comparison of Standards of Spectral Irradiance

A solar irradiance spectrum calculated with the procedure above is only correct if (i) the irradiance scale preserved by the Standards Laboratory providing the lamp is correct, and (ii) the irradiance produced by the lamp when used at a given network site matches the values in the calibration certificate of the lamp. A mismatch can result from a variety of reasons including:

- The 200-Watt lamp became darker or brighter since its calibration at the standards laboratory.
- The irradiance scale preserved by a given laboratory may change over time; i.e. Standards purchased in different years may have different relative calibrations.

- Geometric errors; for example, the distance between lamp and fore-optics does not match the distance specified in the lamp's certificate.
- Thermal effects
- Operator errors

To verify the calibration of the irradiance standards used at the network sites, an engineer from Biospherical Instruments conducts a comparison of all on-site lamps with a "traveling" standard during the annual site visits. Based on these data, we determine if significant changes have occurred. For the 1999-2000 season, each site was equipped with three standards (Historically, there were only two standards).

The comparison of 200-Watt lamps is based on the fact that the spectral irradiance $E_{\text{int}}(\lambda)$, assigned to the internal lamp, should not depend on the 200-Watt lamp used for its calibration. Let us assume for a moment that the internal lamp is calibrated independently with two different 200-Watt standards, lamp #1 and #2. One standard is brighter than the other, and this difference is accurately indicated in the lamps' certificates. In this case, the brighter lamp will lead to a larger PMT current, $I_{\text{ext}}(\lambda)$. The irradiance assigned to the internal lamp, $E_{\text{int}}(\lambda)$, however, will not depend on the 200-W lamp used because the values in the calibration certificate are higher by the same amount. On the other hand, if there is a mismatch between the actual irradiance and the irradiance tabulated in the certificate of a 200-Watt lamp, $E_{\text{int}}(\lambda)$ will depend on the lamp used for the calibration. In more detail, the ratio $C(\lambda)$ between $E_{\text{int}}^{(1)}(\lambda)$, determined with lamp #1, and $E_{\text{int}}^{(2)}(\lambda)$, from lamp #2, allows us to quantify the difference between both calibration standards:

$$C(\lambda) = \frac{E_{\text{int}}^{(1)}(\lambda)}{E_{\text{int}}^{(2)}(\lambda)} = \frac{E_{\text{interp}}^{(1)}(\lambda) \frac{I_{\text{int}}^{(1)}(\lambda, V) - I_{\text{dark}}(V)}{I_{\text{ext}}^{(1)}(\lambda, V) - I_{\text{dark}}(V)}}{E_{\text{interp}}^{(2)}(\lambda) \frac{I_{\text{int}}^{(2)}(\lambda, V) - I_{\text{dark}}(V)}{I_{\text{ext}}^{(2)}(\lambda, V) - I_{\text{dark}}(V)}}$$

Only the definition of $E_{\text{int}}(\lambda)$, determined separately for lamp #1 and #2, was used in the above formula. If lamps #1 and #2 agreed with their certificates, $C(\lambda)$ would be 1. For the intercomparison to be valid, it is important that all scans are performed under the same conditions, i.e., the internal PMT currents $I_{\text{int}}^{(1)}(\lambda, V)$ and $I_{\text{int}}^{(2)}(\lambda, V)$ must be identical, to indicate stability of the internal lamp.

Figure 4.12 shows a comparison of the 200-Watt standards 200W010 (Lamp #1) and M-874 (Lamp #2). Both lamps were calibrated by Optronic Laboratories in September 1998. The comparison was performed on 9/3/97. In Figure 4.12, the function $C(\lambda) - 1$ is depicted. Ideally, the curve should equal the 0% line. In reality, the function deviates by approximately 5% in the UV and by 2% in the visible. Investigation revealed that lamp 200W010 had drifted over time, and that it was darker on 9/3/97 compared to September 1998, when it was (re)calibrated. A darkening of the lamp leads to a smaller $I_{\text{ext}}^{(1)}(\lambda, V)$. If $I_{\text{ext}}^{(1)}(\lambda, V)$ is low, $C(\lambda) - 1$ becomes larger than one, following the equation above. This is in agreement with the result presented in Figure 4.12. If the system had been calibrated with lamp 200W010 rather than M-874, solar irradiance would appear higher.

A lamp drift of 5% within two years is unusually high. Normally, drifts of calibration standards are in the order of <2% per season. Some of the standards, which have been used during Volume 9, have two sets of calibration certificates from Optronic Laboratories, making it possible to track the drift of these lamps over time, see Table 5.2 in the introduction to Chapter 5.

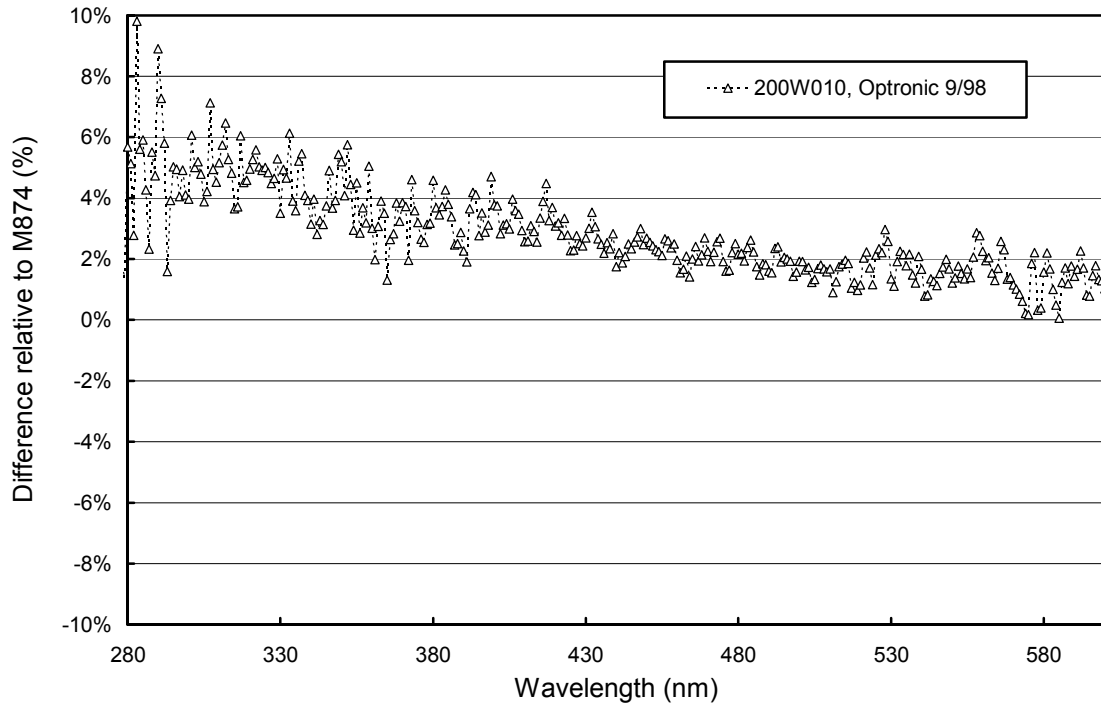


Figure 4.12. Comparison of lamps 200W010 and M-874 expressed by the function $C(\lambda) - 1$. See text for details. The difference relative to M-874 is positive resulting in solar irradiance increasing if 200W010, rather than M-874, were used for calibration.

4.2.1.5. Calibration of Lamps

Not all 200-Watt lamps used in the network have been calibrated by an independent Standards Laboratory. It is therefore necessary to transfer a calibration from a calibrated lamp to other lamps. To calibrate a lamp (i.e. define its scale factor a and color temperature T of the corresponding Black-Body function), lamp and calibrated lamp are operated one after the other and spectral irradiance $E(\lambda)$ of the spare lamp is then calculated by:

$$E(\lambda) = E_{\text{int}}(\lambda) \frac{I(\lambda, V) - I_{\text{dark}}(V)}{I_{\text{int}}(\lambda, V) - I_{\text{dark}}(V)},$$

where $E_{\text{int}}(\lambda)$ is determined with the calibrated lamp as outlined in Section 4.2.1.2. This formula, together with the values obtained from the measurements, gives an appropriate table for $E(\lambda)$ with $290 \text{ nm} < \lambda < 600 \text{ nm}$, which is used to calculate the coefficients a and T for the uncalibrated lamp via a least-square fit. This transfer of the irradiance from reference lamps to other lamps increases the number of calibrated lamps at the sites and also provides backup if the reference standards fail or drift.

4.2.2. Wavelength Calibration and Correction

The wavelength calibration of Volumes 1 - 6 network data was solely based on internal mercury scans (Section 4.2.2.1). Starting with Volume 7, the method has been changed, see Section 4.2.2.2. The prior method is presented here because the results of internal mercury scans are also used in the new approach, although in a different way. Presentation of the original method gives also the rationale for the implemented change.

4.2.2.1. Wavelength Correction with Internal Mercury Scans Implemented for Volumes 1 - 6

The internal low-pressure mercury lamp produces a number of emission lines that are seen as high-intensity, narrow spikes in the wavelength scan (Figure 4.7). The wavelengths of these lines are fixed fundamentally, thus forming the basis of the calibration. The lines are located by scanning in small wavelength steps (0.1 nm) and observing PMT signal changes that are significantly larger than the background noise.

There are different methods for determining the location of a detected peak. The method that was implemented is referred to as the “Tangent” method. It involves extracting several reliable points on each side of a measured maximum from an internal wavelength scan. Seven points on either side of the maximum are used in two linear regressions. The intersection of these two regression lines defines the peak location (Figure 4.13). The reason for using seven points is that the bandwidth of the monochromator is about 0.75 nm, and the number of 0.1 nm readings between two half-maximums of most peaks is seven.

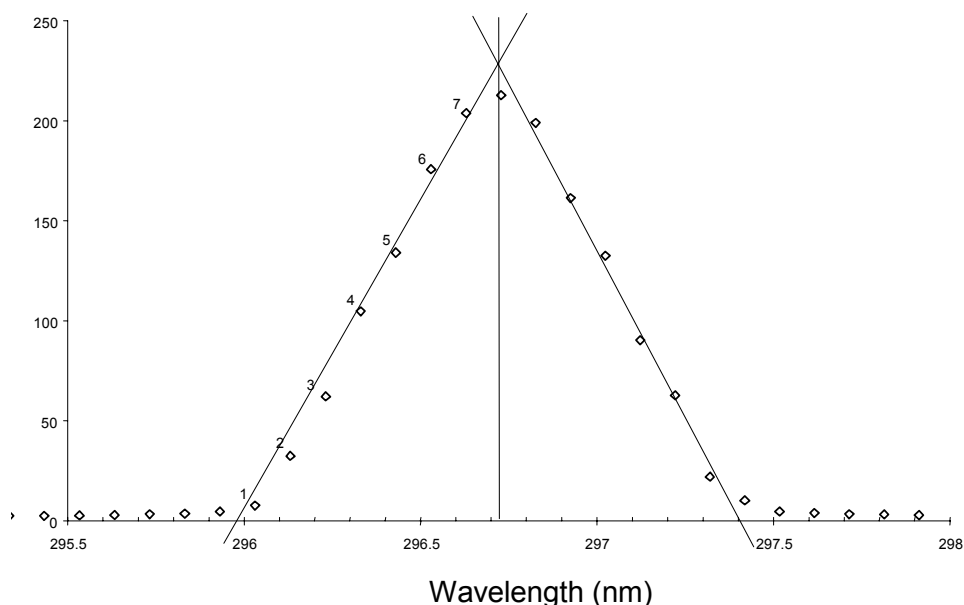


Figure 4.13. *The Tangent method. Diamonds show PMT current of the mercury lamp for the 296-nm peak region. Intersection of the regressions lines defines center wavelength.*

The wavelength correction of data scans recorded in Volumes 1 - 6 was a two-step process. In Step 1, the wavelength shift at the mercury line of 296.73 nm is determined from the daily automatic wavelength scans. By subtracting this wavelength from the true wavelength, 296.73 nm, the wavelength shift is determined. This shift is then applied to the solar scans, i.e., the whole spectrum is shifted by a single constant value. After this step, the spectrum would be aligned correctly at 296.73 nm if the calibration with internal mercury scans were without errors. Due to non-linearities in the monochromator’s wavelength drive, however, this will not provide a correct wavelength alignment for the whole spectrum.

In Step 2 of the procedure, a shift-function is applied that is calculated from 13 mercury lines of the wavelength scan. This function corrects for monochromator non-linearities. An example of this function is shown in Figure 4.14. The function is zero at 296.73 nm because it only describes wavelength deviations between measured and nominal wavelength positions relative to this wavelength. The function is usually very stable throughout a season and is therefore calculated from the average of all wavelength scans performed during that season. The function is described by a series of linear equations of the form $\Delta\lambda = a_n + b_n\lambda$ (the constants a_n and b_n are offset and slope) that are determined stepwise for peak-to-peak wavelength segments.

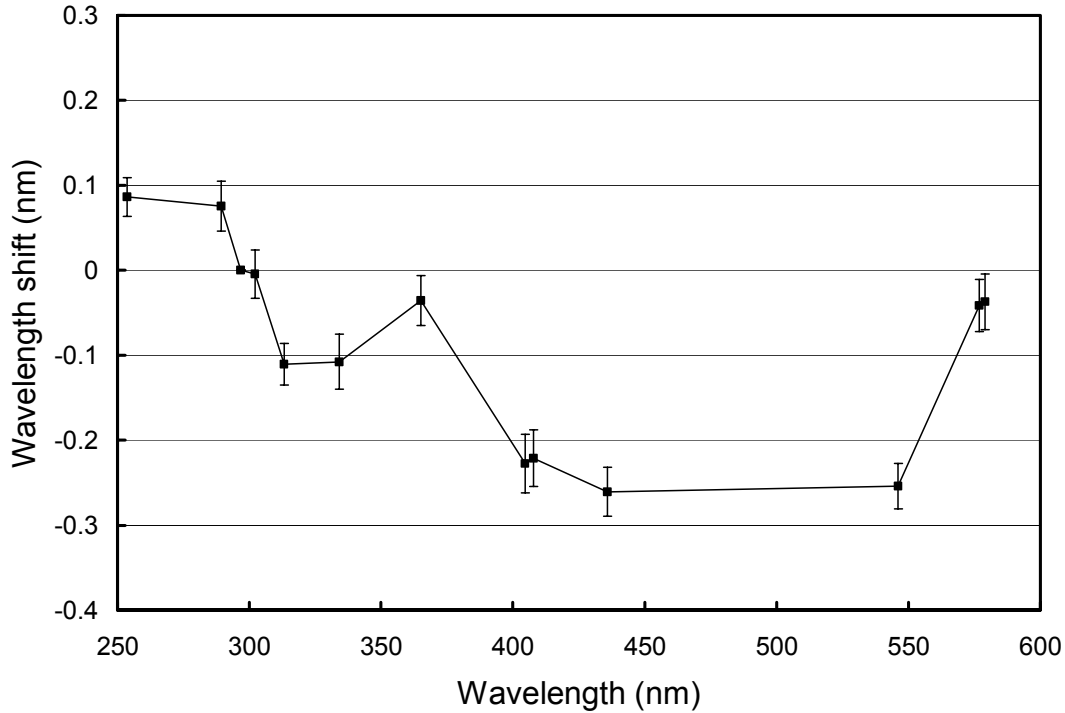


Figure 4.14. Typical monochromator non-linearity. Approximately 347 internal wavelength scans were evaluated. The error bars represent $\pm 1\sigma$ limits calculated from these scans.

In summary, Step 1 takes account of the day-to-day wavelength fluctuations by aligning a spectrum to 296.73 nm, and Step 2 corrects for monochromator non-linearities that remain fairly constant throughout a season.

From an examination of the approximately 300-400 mercury scans typically recorded during a season, **three sources** of uncertainty in the wavelength alignment appear.

First, there may be wavelength fluctuations within one day, which cannot be detected by wavelength scans that are usually performed only once a day. These variations can be attributed to power failures, loss of index in the stepping motor, thermal expansion of the monochromator due to temperature variations, other mechanical causes, and random noise in the peak-finding algorithm. Typically, the variation in the position of the 296.73-nm line is less than ± 0.02 nm between consecutive wavelength scans and this value is therefore also a good estimate of the wavelength variation during one day. Figure 4.15 shows a typical distribution of the wavelength deviation from the 296.73-nm line. The figure is based on all wavelength scans performed during a season.

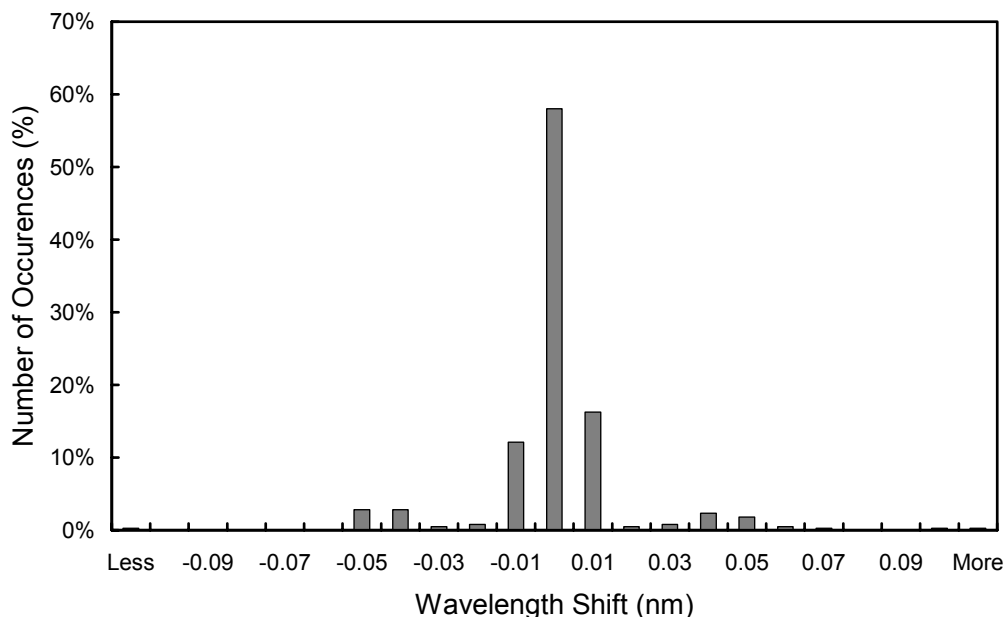


Figure 4.15. Typical differences in the measured position of the 296.73 nm mercury line between consecutive wavelength scans. The x-labels give the center wavelength shift for each column. Thus, the 0-nm histogram column covers the range -0.005 to +0.005 nm. “Less” means shifts smaller than -0.105 nm; “more” means shifts larger than 0.105 nm. For 88% of the days, the change in offset is smaller than ± 0.025 nm.

The **second** source of uncertainty is caused by changes in monochromator non-linearity during a season. Usually only one function is applied for the season. (Occasion requires sometimes that two or three functions have to be applied. This is usually necessary if a monochromator has to be serviced or replaced during a season). The uncertainty caused by this approach is given by the standard deviation of the variation of individual wavelength scans. In the UV-B, the standard deviation (1σ) is generally less than 0.01 nm, and increases to 0.05 nm in the visible. The uncertainty in the UV-B is lower because most of the fluctuations are removed by Step 1 described above.

A **third** source of error in the wavelength domain occurs due to the different optical light paths for internal wavelength scans and measurements of solar irradiance. This effect can be tracked by comparing internal and external wavelength scans. The different geometry introduces a bias into the data that is usually constant throughout an operating season but varies slightly from site to site. For example, during the 1996-1997 season, external wavelength scans were performed during site visits at all sites. While these scans exhibit consistent results at the beginning and end of the season, variations from site to site were as much as 0.05 nm, as measured by the offset of the 296.73 nm spectral line. The difference in the 296.73-nm line offset, calculated from external and internal wavelength scans, was 0.1 nm for Ushuaia and Palmer, and 0.14 nm for the South Pole. Figure 4.16 shows how the difference between both scan types may depend on wavelength. The difference at 296.73 nm is about 0.1 nm, increases to about 0.13 nm at 400 nm, and is about 0.05 nm in the visible.

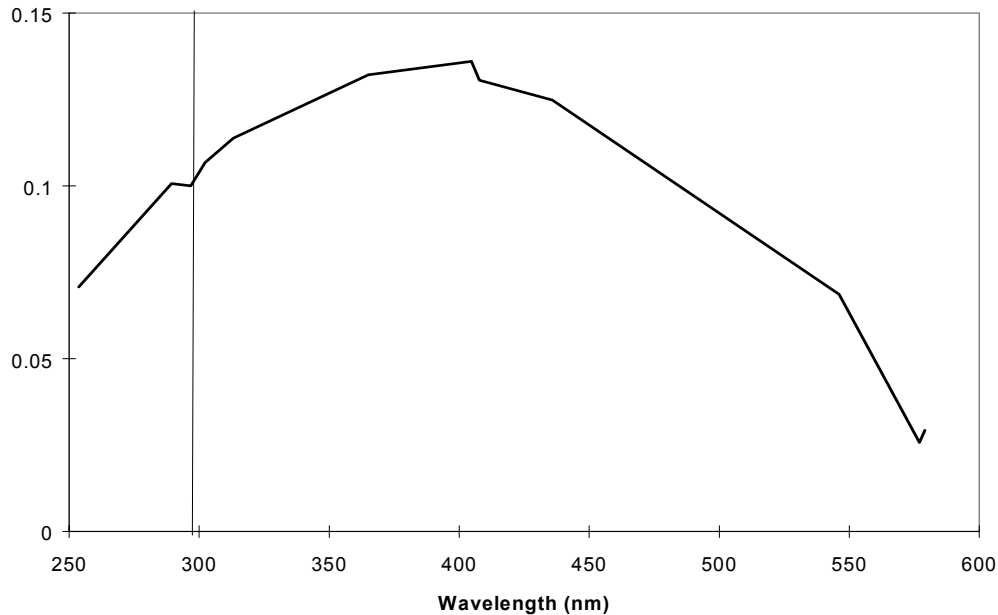


Figure 4.16. Typical difference between the monochromator corrections based on external and internal mercury scans. The vertical line emphasizes the difference at 296.73 nm.

This bias has not been corrected in Volume 1 through 6 data. Starting with Volume 7, the problem has been addressed by implementing a method described in the next section. In order to give data users a feeling of how much the data have been affected in the past, a subset of San Diego Volume 7 data has been wavelength corrected with both the historic and new methods. A comparison of both datasets is compiled at the end of the Section 4.2.2.2.

4.2.2.2. Wavelength Calibration and Correction by the Fraunhofer-Correlation Method Implemented for Volume 7 – 9 Data

Principle of the correlation method

In order to improve the accuracy of the wavelength calibration and to avoid the problems associated with internal mercury scans, a new methodology was implemented for Volume 7 and 9. The method utilizes the Fraunhofer structure in solar spectra, which is caused by absorption processes in the Sun's outer atmosphere. This structure is also very marked in spectra of solar irradiance measured with the SUV-100 network radiometers, see for example Figure 4.3. By correlating the structure in measured spectra with a similar structure in a reference solar spectrum (i.e., a spectrum with negligible wavelength errors) the wavelength shift can be determined and the measured spectra corrected. The method applied here is based on an implementation suggested by Slaper et al. (1995), Slaper (1997), and Slaper and Koskela (1997). The correlation-software (SHICrvm Version 2.7.) was provided by H. Slaper and was extended appropriately to match the data format and processing requirements of the NSF Network. The reference solar spectrum is based on a high-resolution (< 0.001 nm) extraterrestrial spectrum measured by the Fourier-Transform Spectroradiometer (FTS) at the National Solar Observatory (NSO) located at Kitt Peak, Arizona (Kurucz et al., 1984). The original spectrum was slightly modified by H. Slaper to account for an erroneous peak in the Kitt Peak spectrum in the 320-330 nm range (Slaper and Koskela, 1997). The wavelength accuracy of this spectrum has been proven to be better than 0.003 nm. The method has been successfully used to evaluate the results of several European intercomparison campaigns (Slaper et al., 1995; Slaper, 1997; Slaper and Koskela, 1997; Reinen et al., 1998; Seckmeyer et al., 1998).

Fraunhofer-correlation method compared to wavelength alignment with external wavelength scans

Alternative to the Fraunhofer-correlation method outlined above external mercury scans could have been used to improve the wavelength accuracy. For the following reasons we decided to use the correlation method:

1. In our implementation of the Fraunhofer-correlation method a wavelength shift value is provided every 10 nm between 300 and 440 nm giving 15 values in total. There are only four useable mercury lines in the same spectral range. Thus the correlation method delivers corrections in much smaller wavelength intervals. Since some monochromators deployed in the network show variations in linearity varying on a 20-nm scale, the higher resolution of the correlation method improves overall correction accuracy.
2. Only a few external wavelength scans exist as these scans are only performed during a site visit. With the correlation method, the wavelength accuracy can be checked every day or even every scan, allowing to analyze drifts during a particular day.
3. Peaks from external wavelength scans are asymmetrical. Depending on the method applied, the center wavelength assigned to such a scan may vary by up to 0.15 nm.
4. For the correlation method, we assume a symmetrical, triangular slit function with the same bandwidth as is typical for external wavelength scans of the site under consideration. Published data of spectral irradiance can therefore be used as if the actual slit function were symmetrical. Therefore data users do not have to correct for asymmetry effects by themselves.
5. The correlation method uses the Sun as the calibration source. Therefore, the calibration source is the same for all sites, resulting in consistent wavelength calibrations at all sites.

Implementation of the correlation method

The objective of the implementation is to define the monochromator non-linearity correction function. The set of linear functions presented in Section 4.2.1.1 is replaced by a set of similar functions derived from the Fraunhofer-correlation method.

The Fraunhofer-correlation method can be used only in the wavelength range between 300 nm (310 nm for Barrow, McMurdo, and South Pole due to low solar elevations) and 440 nm. Below 300 nm, the signal is too noisy, i.e., the Fraunhofer structure in measured spectra is too distorted by noise to allow a reasonable correlation with the reference spectrum. Above 440 nm, the accuracy of the available reference spectrum is unknown and therefore we decided not to implement the method there.

In order to retrieve correction values outside the range of 300-440 nm we applied a combination of internal wavelength scans and the Fraunhofer-correlation method. In the first step, the mean deviation of wavelength shifts determined with internal wavelength scans and the Fraunhofer-correlation method is determined between 300 and 440 nm. For all sites the mean difference is between 0.08 and 0.15 nm, which is also consistent with the difference between internal and external wavelength scans. In a second step, the values of the internal wavelength scans outside the 300-440 nm range are shifted by this average value. We estimate the accuracy of this method for wavelengths in the critical region around 300 nm to be better than 0.05 nm. For example, the shift values for the two neighboring wavelengths 300 nm (Fraunhofer-based) and 296.73 nm (based on shifted internal wavelength scan) usually agree to within 0.03 nm. For wavelengths above 440 nm, the wavelength accuracy is less critical for the applications we are aware of.

The algorithm used to calculate the monochromator non-linearity correction functions consists of six steps:

1. Determine the wavelength shift of the 296.73 nm mercury line from the daily internal wavelength scans and apply this shift to the data scans. Step 1 is similar as for the method described in Section 4.2.1.1, where the wavelength correction was solely based on internal scans. After this step, all data scans are aligned consistently at 296.73 nm. Due to the bias of internal wavelength scans there is still

an error in the wavelength alignment at 296.73. Step 1, however, is only intended to homogenize the data set (i.e., remove day-to-day fluctuations) rather than eliminate the systematic bias.

2. Use the Fraunhofer-correlation algorithm to determine the wavelength-dependent wavelength shift in the homogenized data set (300-440 nm).
3. Compare the wavelength-shifts determined with the Fraunhofer-correlation method with the shifts apparent in internal mercury scans, calculate the mean deviation, and shift the values from the internal wavelength scans *outside* the core-interval (i.e., $\lambda < 300$ nm or $\lambda > 440$ nm) by this shift value.
4. Establish a set of linear equations describing the monochromator non-linearity function. Usually, only one function is needed per site and season.
5. Apply the wavelength correction to all data.
6. Check the result of the wavelength correction by running the Fraunhofer-correlation method again.

Figure 4.17 illustrates two functions expressing the monochromator non-linearity that were determined for the Barrow instrument. The lower curve is based on the original method, i.e., only internal mercury scans have been evaluated. The upper curve was generated with the new Fraunhofer-correlation method. As described above, a pure Fraunhofer correlation was applied in the core range of 310-440 nm and the values outside this range are based on shifted internal scans. The difference between both curves is about 0.12 nm. The graph is based on data from the current 1997-98 season and the upper curve represents the correction function that was actually applied to the Barrow data of this season. Using one function for the whole season is justified because monochromator non-linearities were very stable throughout the year, as indicated by the error bars in Figure 4.17. These represent the 2σ standard deviation of the monochromator non-linearity and were calculated from all noontime scans recorded during the season.

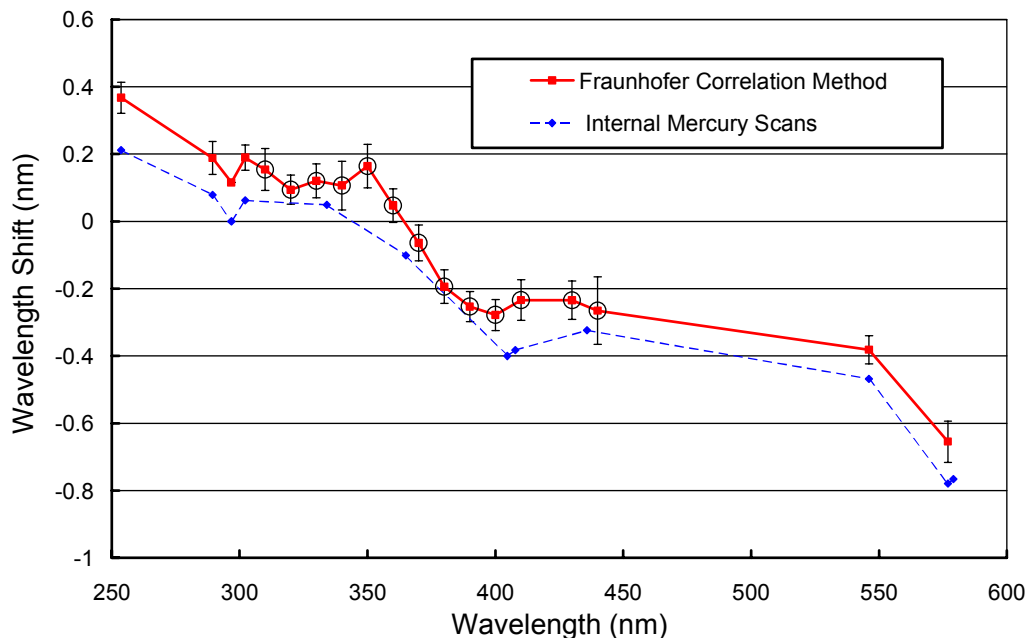


Figure 4.17. Monochromator non-linearity correction function for Barrow Volume 7. Dashed line: Function calculated solely with internal mercury scans. Solid line: Function calculated with a combination of results from the Fraunhofer-correlation method and internal mercury scans. Between 310 and 440 nm the function is based on the Fraunhofer-correlation method only (marked with circles in the plot). Outside this interval, the function is based on internal mercury scans, which were shifted by the mean difference between both methods. See text for a more detailed description. Both functions represent average wavelength shifts for the 1997-98 season. The error bars give the 2σ standard deviation variation of the wavelength shifts.

Quality control of the Fraunhofer correlation method

After the data were corrected, the residual wavelength shifts were again determined with the Fraunhofer-correlation algorithm. The result is shown in Figure 4.18. For wavelengths between 320 and 440 nm, the shift is generally smaller than ± 0.1 nm, with a few exceptions. The 310 nm shifts show a larger deviation in 1997 and early in 1998. However, these more pronounced shifts are not due to the instrument. At these parts of year, solar zenith angles are rather large and measurements at 310 nm are only slightly above the detection limit. Thus the correlation method is affected by noise in the solar data leading to erroneous results.

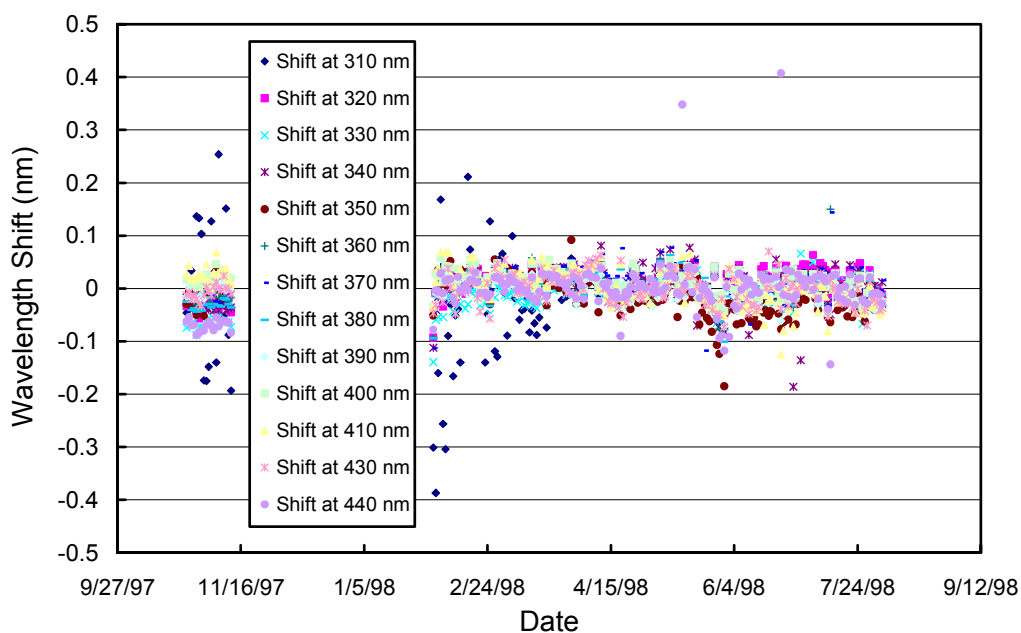


Figure 4.18. Check of the wavelength alignment of the Barrow Volume 7 data after applying the Fraunhofer-correlation-based wavelength correction. The check was performed with the method developed by Slaper et al. (1995) using noontime spectra from the 1997-98 season. Similar results have been obtained for all sites and also for Volume 9 (see Section 5).

The check of the wavelength alignment presented in Figure 4.18 is not a complete evaluation of the absolute wavelength accuracy of the Barrow 1997-98 data. Both the calculation of the correction function and the check after applying the correction were performed with the same algorithm based on the work of Slaper et al. (1995). Therefore the wavelength alignment can be still affected by systematic errors introduced by this algorithm or its reference spectrum. According to Slaper and Koskela (1997), the estimated alignment uncertainty of the method is “probably less than 0.02 nm for instruments with a FWHM of 1 nm or less.” However, features in the measured spectra, which are not caused by the Fraunhofer structure (e.g., changes in the wavelength increment and pauses when the PMT high-voltage changes), may confuse the algorithm. We therefore also checked the wavelength-corrected data set with an independent implementation of a Fraunhofer-correlation method that had been developed by Mayer (1997). The reference spectrum of this method is an extraterrestrial spectrum measured by the Solar Ultraviolet Spectral Irradiance Monitor (SUSIM) during the third space shuttle mission of the Atmospheric Laboratory for Applications and Science (ATLAS 3). The original spectrum can be obtained from the ftp server <ftp://susim.nrl.navy.mil>. The spectrum is given in vacuum-wavelengths and was shifted to air-wavelength before its use in the correlation algorithm.

Figure 4.19 shows the result of the check with the method developed by Mayer (1997). Between 310 and 400 nm, the deviations are smaller than ± 0.1 nm with only few outliers. As expected, the wavelength shifts are slightly larger than those presented in Figure 4.18. Deviations of both methods of about 0.02 nm have also been reported by Seckmeyer et al. (1998). The deviations are still sufficiently small to give confidence

in the wavelength correction. We therefore have implemented the Fraunhofer-correlation method at all sites for Volume 7 - 9 data.

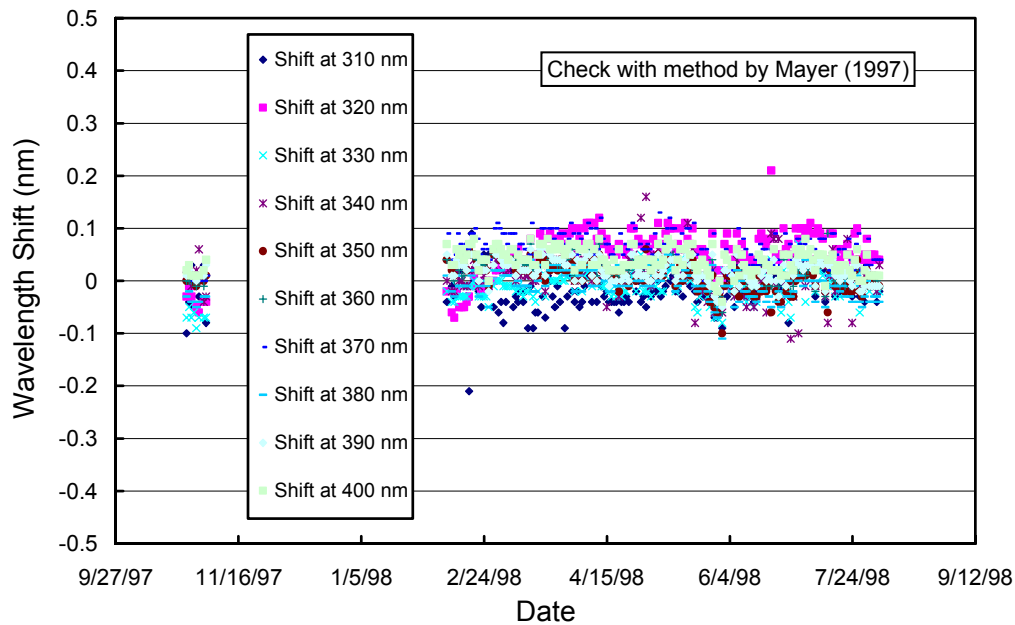


Figure 4.19. Check of the wavelength alignment of the Barrow Volume 7 data after applying the Fraunhofer-correlation-based wavelength correction. The check was performed with the method developed by Mayer (1997).

Comparison of the historic wavelength correction method with the Fraunhofer-correction method

In order to quantify the effect of the change in the wavelength correction method on solar irradiance data, a subset of San Diego Volume 7 data (days 9/9/97-12/31/97) was corrected with both the historic and the new procedures. Figure 4.20 shows the ratio “historic correction/new correction” for several irradiance integrals versus solar zenith angle. The difference in both datasets depends significantly on wavelength. For example, the integral 400-600 nm is almost independent of the wavelength correction applied (i.e., the ratio is about 1.0), while differences for the 303.03-307.692 nm integral can be as high as 6.5%. This behavior can be expected because the latter integral includes wavelengths in the UV-B, where ozone absorption leads to a large change of spectral irradiance with wavelength. The ratio for this short-wave UV-B integral is always smaller than 1.0. This means that a wavelength correction with the historic method, which was applied for Volume 1-6 data, leads to lower irradiances than a correction with the Fraunhofer method. This can also be concluded from the direction of the shift between internal and external mercury scans.

Figure 4.20 also includes a comparison of both correction methods for two biological dose-rates, erythemally weighted irradiance and DNA-weighted irradiance. At 50° SZA, values corrected with the old method are lower by 2% and 4% for erythemal and DNA irradiance, respectively. For DNA-weighted irradiance, the difference is almost independent of SZA, whereas the difference for erythemal values appears to be smaller at larger SZA. This SZA-dependency is quite different from the behavior of the 303.03-307.692 nm integral mentioned earlier. For this integral, the difference at 30° SZA is about 4%. At 75° SZA, the difference increases to 6.5% and then diminishes again towards larger SZAs. The reason for this change with SZA is the different “shape” of the solar spectrum at different solar elevations.

The magnitude of the difference between both correction methods agrees very well with theoretical evaluations published by Bernhard and Seckmeyer (1999). In this paper, formulas are given to calculate the effect of wavelength shifts on biologically weighted irradiance as well as on spectral irradiance at a

specific wavelength. The formulas require as input parameters the magnitude of the wavelength shift, SZA, total column ozone, and the action spectrum under consideration. We applied these formulas to San Diego data by setting the wavelength shift to 0.109 nm (the average difference between internal and external wavelength scans for the San Diego instrument in late 1997), and total column ozone to 300 DU (approximately the average total column ozone for San Diego). The results are indicated in Figure 4.20 with large symbols. As can be seen, the theoretical results fit well to the experimental data, both in magnitude and SZA-dependency. For example, the increase of the ratio “historic correction / new correction” for erythemal irradiance towards larger SZA is also reflected in theoretical results (compare small and large diamond symbols in Figure 4.20). Similarly, the bowl-shaped ratio of the 303.03-307.692 nm integral is confirmed by the theoretical values (square symbols).

The data presented in Figure 4.20 are from San Diego only and may not be representative for high latitude sites, where total column ozone is quite different from the prevailing values for San Diego. This is particularly the case in September and October when the ozone hole affects measurements at the austral sites. According to Bernhard and Seckmeyer (1999), however, the influence of column ozone on systematic errors in biologically weighted irradiances caused by wavelength shifts is usually below 0.5%. The results from San Diego can therefore also be applied to the other network sites.

In conclusion, biological dose-rates published in earlier volumes appear to be too low by approximately 2-4%, almost independent on solar zenith angles, if the same shift between “internal” and “true” wavelength existed as for the San Diego instrument. The systematic errors in short-wave UV-B irradiances, like the 303.03-307.692 nm integral, may be larger and, in addition, SZA-dependent. On the other hand, integrals in the UV-A and visible are insignificantly affected by the systematic error introduced by the historic wavelength correction method, which was based on internal mercury scans only.

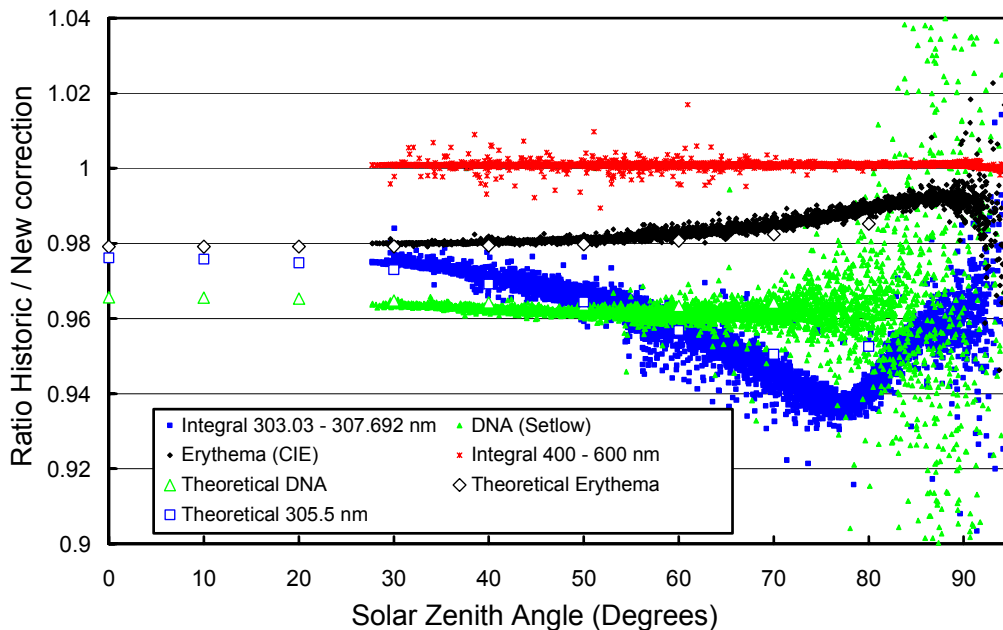


Figure 4.20. Effect of the wavelength correction method on spectral integrals. Small symbols show the ratios of data, which were corrected with the historic mercury scan based method, to data corrected with the new Fraunhofer method. Four different data products are depicted, including the 303.03-307.692 nm and 400-600 nm integrals, as well as erythemally and DNA-weighted irradiance. Large symbols show theoretical results according to Bernhard and Seckmeyer (1999). See text for details.

4.2.3. Biological Dose-Rate Calculations

The impact of radiation on biological systems is usually described as the integral of the product of spectral irradiance, $E(\lambda)$, and a "biological weighting function" $W(\lambda)$:

$$E_{\text{bio}} = \int_{\lambda_1}^{\lambda_2} E(\lambda)W(\lambda) d\lambda$$

$W(\lambda)$ is also often denoted "action spectrum" and is a dimensionless function. In this report, we refer to E_{bio} usually as a "biological dose-rate." (Integrating biological dose-rate over time results in a "biological dose", see Section 4.2.4). Spectral data from the UV network are routinely processed to calculate biological dose-rates according to several published weighting functions. The above integral is usually evaluated with the integration limits, 286 and 400 nm, respectively. The integration is approximated via a sum with $d\lambda = 0.2$ nm steps typically between 286 and 345 nm, and $d\lambda = 0.5$ nm steps between 345.0 and 400 nm, where applicable.

The published data include six biological dose-rates abbreviated Setlow, Hunter, Caldwell, Dose1, Dose2, and Dose3_CIE_Erythema. The action spectra for these dose-rates are described below and are plotted in Figure 4.21 and Figure 4.22. The data of spectral irradiance were also weighted with the spectral responsivity of the TSI sensor (Figure 2.6) and also published. Please see the Appendix for a detailed listing of the code used to compute biological dose-rates from these weighting functions.

"Setlow" is based on a parameterization of the spectral dependence of damage to unprotected DNA that was suggested by R. B. Setlow (1974). The integration range is from 286 to 340 nm.

$$W(\lambda) = 10^{D(\lambda)}, \text{ where } D(\lambda) = \begin{cases} 13.04679 - 0.047012\lambda, & 286 \leq \lambda < 290 \\ 20.75595 - 0.073595\lambda, & 290 \leq \lambda < 295 \\ 30.12706 - 0.105362\lambda, & 295 \leq \lambda < 300 \\ 42.94028 - 0.148073\lambda, & 300 \leq \lambda < 305 \\ 45.24538 - 0.15563\lambda, & 305 \leq \lambda \leq 340 \end{cases}$$

Please note that other parameterizations of Setlow (1974) exist. Care must be used when results of different implementations are compared.

"Hunter" is based on an exponential function fit to the data of J.H. Hunter, J.H. Taylor, and H.G. Moser (1979) and reported in numerical form by R.C. Smith and K. S. Baker (1982). The integration range is from 290 to 340 nm.

$$W(\lambda) = \exp\{61.1381 - 0.21551\lambda\}$$

"Caldwell" refers to a parameterization of A.E.S. Green, T. Sawada, and E.P. Shettle (1974) for Caldwell's data on the relative photon effectiveness of UV-B irradiation to induce biological response, when protein or nucleic acid chromophores are involved (M. M. Caldwell, 1971). Integration range is from 286 to 313 nm.

$$W(\lambda) = 2.618 \cdot \left(1 - \left(\frac{\lambda}{313.3}\right)^2\right) \cdot \exp\left\{\frac{300 - \lambda}{31.08}\right\}$$

"Dose1" refers to an action spectrum of erythema defined by W.D. Komhyr and L. Machta (1973). The parameterization used is found in A.E.S. Green, T. Sawada, and E.P. Shettle (1974). The weighting function peaks at 296.5 nm. The integration range is 286 to 400 nm. Note that a coding error exists in previous data sets (Volume 1-5) for this action spectrum; for more information see the Errata Section of the Appendix.

$$W(\lambda) = \frac{0.4485}{1 + \frac{\exp\{\lambda - 311.4\}}{3.13}} + \frac{4 \cdot 0.9949 \cdot \exp\left\{\frac{\lambda - 296.5}{2.692}\right\}}{1 + \exp\left\{\frac{\lambda - 296.5}{2.692}\right\}^2}$$

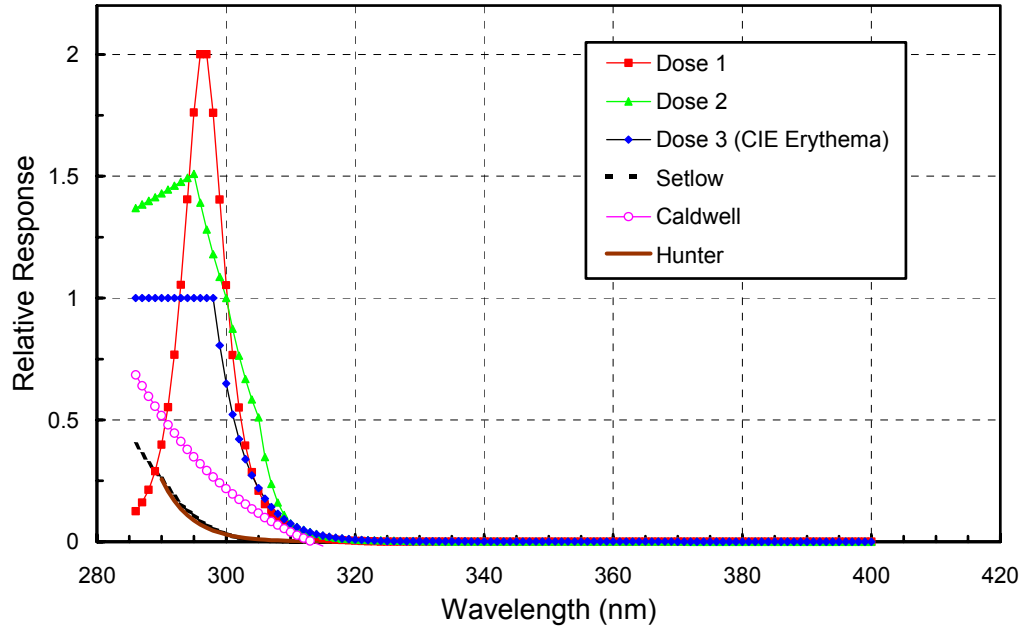


Figure 4.21. Biological weighting functions used to calculate biological dose-rates from spectral irradiance data.

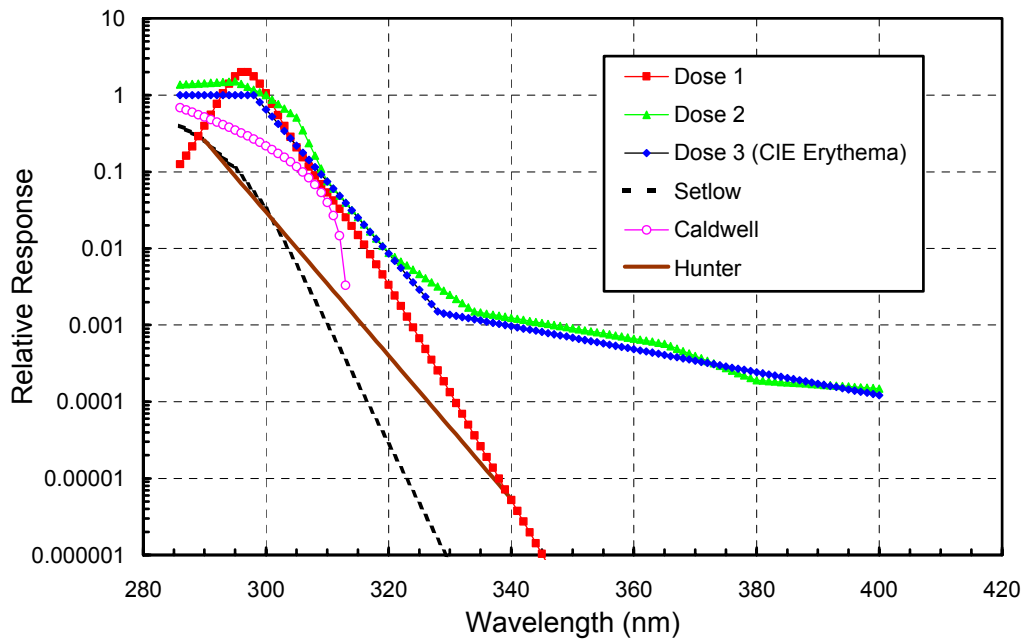


Figure 4.22. Biological weighting functions as in Figure 4.21 but plotted on a logarithmic y-axis.

"Dose2" refers to an alternative action spectrum for erythema in human skin proposed by B.L. Diffey (1987). It is a multisegment power fit to tabular data.

$$W(\lambda) = 10^{D(\lambda)}, \text{ where } D(\lambda) = \begin{cases} -1.215837 + 0.004728\lambda, & 286 \leq \lambda < 295 \\ 10.73862 - 0.035795\lambda, & 295 \leq \lambda < 300 \\ 17.54579 - 0.058486\lambda, & 300 \leq \lambda < 305 \\ 50.49061 - 0.166502\lambda, & 305 \leq \lambda < 310 \\ 27.87686 - 0.093554\lambda, & 310 \leq \lambda < 320 \\ 15.3893 - 0.054531\lambda, & 320 \leq \lambda < 335 \\ 1.703584 - 0.013555\lambda, & 335 \leq \lambda < 365 \\ 8.365825 - 0.031808\lambda, & 365 \leq \lambda < 380 \\ -1.705338 - 0.005305\lambda, & 380 \leq \lambda \leq 400 \end{cases}$$

Please note that this function peaks at 295 nm $\max[W(\lambda)] = 1.51$.

"Dose3_CIE_Erythema" refers to the action spectrum for erythema in human skin proposed by McKinlay and Diffey (1987). This is the erythema action spectrum that is most widely used and it is often referred to as the "CIE action spectrum for erythema."

$$W(\lambda) = 10^{D(\lambda)}, \text{ where } D(\lambda) = \begin{cases} 0, & 286 \leq \lambda < 298 \\ -0.094(\lambda - 298), & 298 \leq \lambda < 328 \\ -0.015(\lambda - 139), & 328 \leq \lambda \leq 400 \end{cases}$$

Note that this function equals "1" below 298 nm.

"Weighted TSI" is obtained by weighting spectral irradiance with the spectral responsivity of the TSI sensor. The sensor consists of a filtered photodiode. The responsivity function was calculated from spectral transmission of the filter and spectral response of the diode. The integration range is 320 to 392 nm and the function is parameterized as follows:

$$W(\lambda) = \begin{cases} 0.005598382 - 0.04901834 \frac{\lambda}{1000} + 0.1420638 \left(\frac{\lambda}{1000}\right)^2 - 0.1361036 \left(\frac{\lambda}{1000}\right)^3, & \lambda < 367 \\ -0.08228739 + 0.6492523 \frac{\lambda}{1000} - 1.70513 \left(\frac{\lambda}{1000}\right)^2 + 1.490757 \left(\frac{\lambda}{1000}\right)^3, & \lambda \geq 367 \end{cases}$$

4.2.4. Calculation of Daily Doses

Daily doses are calculated by integrating instantaneous irradiance values over time:

$$D = \int_{x-12}^{x+12} E(t) dt$$

Here E symbolizes either dose-rates or irradiance integrated over a specific wavelength range, for example spectral irradiance, integrated over 400-600 nm. The integration range is centered at local apparent noon x (01:00 GMT for McMurdo, 16:00 GMT for Palmer, 12:00 GMT for South Pole, 17:00 GMT for Ushuaia, 20:00 GMT for San Diego, and 22:00 GMT for Barrow). For example, the integration period for McMurdo is from 13:00 GMT of the preceding day until 13:00 GMT of the current day.

The integration is affected by gaps in the data and the fact that the first and last measurement of a given day usually occur during times when light levels are already significantly above zero. Therefore, interpolation and extrapolation of the measured data set is necessary before the integration can be performed. This is done by fitting a spline curve through the measured data points. The procedure is explained with Figure 4.23.

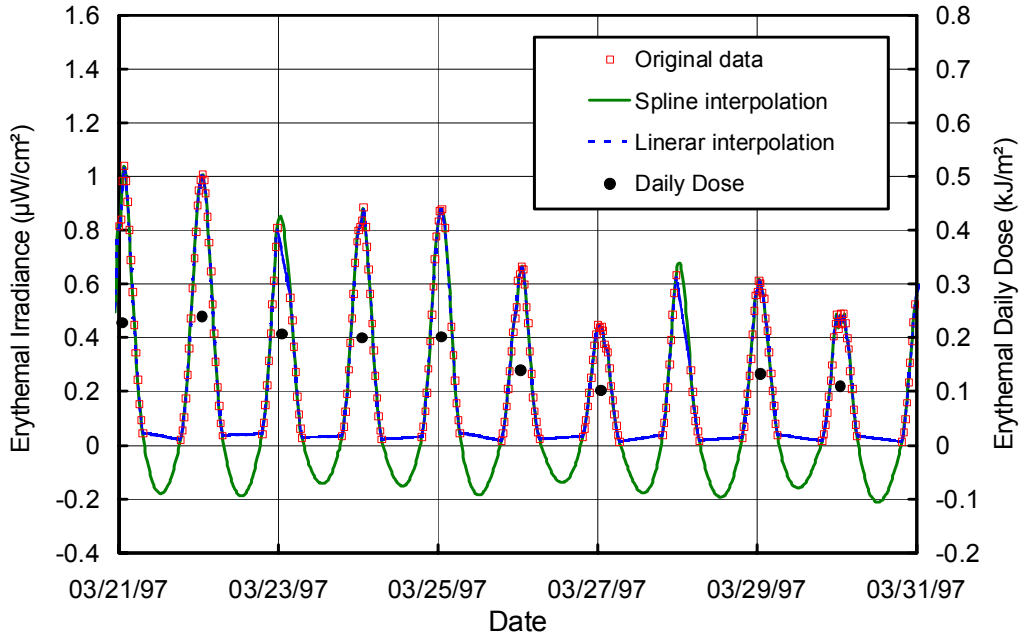


Figure 4.23. Explanation of procedure to calculate daily doses. Squares: Measured erythemally weighted irradiance (left axis). Solid line: Spline interpolation of measured data. Broken line: Linear interpolation. Filled circles: Calculated erythemal daily dose (right axis).

It can be seen from Figure 4.23 that the spline-interpolated curve fills gaps in measured data in a reasonable fashion. In particular when measurements are missing around noon-time (e.g. 3/23/97 and 3/28/97), spline-interpolation is superior to linear interpolation (compare solid and broken lines in Figure 4.23). When the spline-curve is negative, values are set to zero. So the calculated daily dose is proportional to the area limited by the zero-line and the spline-curve. When gaps in data are too large the calculation of daily doses is clearly not appropriate. The time limit is set to 15000 seconds. Daily doses for days which larger gaps (like 3/28/97) are not reported in the published data.

4.2.5. Calculation of Solar Zenith and Azimuth Angles

All data in the databases on CD-ROM are accompanied with solar zenith and azimuth angles at the middle of a data scan. Both angles were calculated according to an algorithm presented by Wilson (1980).

